Inorganic Chemistry
Cite This: Inorg. Chem. XXXX, XXX, XXX−XXX
Article
pubs.acs.org/IC

$Cs_3RE^{III}Ge_3O_9$ (RE = Pr, Nd, and Sm−Yb) and $Cs_8Tb^{III}_2Tb^{IV}Ge_9O_{27}$: A Rare Example of a Mixed-Valent Tb(III)/Tb(IV) Oxide

Gregory Morrison,[†,§] Nicholas R. Spagnuolo,[†,§] Stavros G. Karakalos,[‡] and Hans-Conrad zur Loye*[,†]

[†]Department of Chemistry and Biochemistry and [‡]Department of Chemical Engineering, University of South Carolina, Columbia, South Carolina 29208, United States

Supporting Information

ABSTRACT: Single crystals of 12 new cesium rare earth germanates crystallizing in two new structure types were grown from a CsCl/CsF flux. $Cs_3REGe_3O_9$ (RE = Pr, Nd, and Sm−Yb), a new family of germanates that form for almost the entire series of rare earth elements, crystallizes in orthorhombic space group $Pna2_1$ with lattice parameters in the following ranges: a = 13.7033(4)−14.022(2) Å, b = 7.0545(2)−7.2405(12) Å, and c = 12.6672(4)−12.836(2) Å. Surprisingly, the Tb reaction yielded both $Cs_3TbGe_3O_9$ and $Cs_8Tb_3Ge_9O_{27}$, a rare example of a mixed-valent Tb(III)/Tb(IV) compound. $Cs_8Tb_3Ge_9O_{27}$ crystallizes in space group $P3$ with the following lattice parameters: a = 11.2906(4) Å, and c = 7.9605(3) Å. The mixed-valent oxidation state of Tb was confirmed by structure solution, bond-valence sums, X-ray photoelectron spectroscopy data, and magnetic data. Optical and magnetic properties are reported for both sets of compounds.

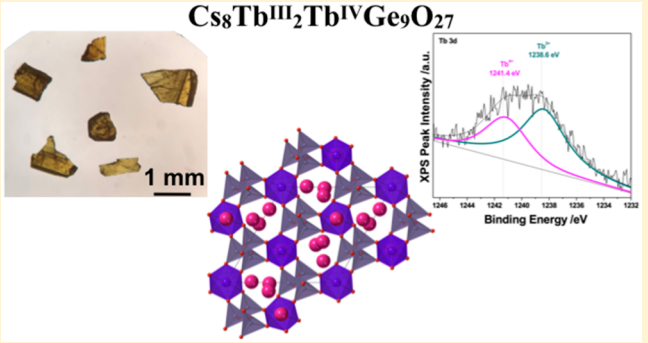

INTRODUCTION

Rare earth silicates make up an extensively studied class of materials that have attracted attention due to their potential applications, primarily as optical and luminescent materials.[1−8] The rare earth germanates, while offering the same potential applications,[9] are considerably less studied. In many cases, the germanates adopt the same structures as the corresponding silicates.[10−12] However, in some instances, new structure types and even compositions exist for the germanates that are not known for the silicates.[13] The 12 cesium rare earth germanates reported in this work crystallize in two new structure types with no analogous silicate compositions.

Typically, the rare earths adopt the +3 oxidation state in oxides. The most common exceptions to this are cerium, which readily oxidizes to a +4 state under oxidizing conditions,[13−15] and europium, which can be reduced to a +2 state in flux growth reactions by metal reducing agents such as Zn.[16] The latter case, Eu(II), occurs due to the resulting half-filled 4f subshell. Terbium(IV) also contains a half-filled 4f subshell but is typically considered quite oxidizing in nature and is not usually obtained under common synthetic conditions.[17] Besides TbO_2,[18] few other examples of Tb(IV) oxides exist and are mostly perovskites and related materials.[19−21] Typically, these are produced via solid-state reactions at high temperatures (1300 °C)[21] and/or under an O_2 atmosphere[20] to achieve the Tb(IV) state. A non-perovskite-related Tb(IV) oxide, $K_2TbGe_2O_7$, was obtained under hydrothermal conditions through the reaction of Tb_4O_7 and GeO_2 in the presence of 20 M KOH as a mineralizer.[17]

As uncommon as Tb(IV) oxides are mixed Tb(III)/Tb(IV) compounds. A limited number of mixed-valent terbium fluorides have been achieved through the thermal decomposition of TbF_4.[22−25] For the oxides, a series of binary phases exists between Tb_2O_3 and TbO_2,[26−28] with "Tb_4O_7", a mixture of Tb_7O_{12} and $Tb_{11}O_{20}$, being the most commercially available terbium oxide. Few higher-order Tb(III)/Tb(IV)-containing oxides are known.[29]

We have been exploring the rare earth germanate phase space via flux growth.[12,13,30,31] In particular, we have found mixed alkali halide fluxes to be particularly well suited for the synthesis of alkali rare earth germanates.[12,13] Recently, we reported on the synthesis and structures of Ce(IV) germanates crystallizing in the Wadeite structure type[32] and two Dy(III) germanates that crystallize in related structures.[13] In our continued exploration of this phase space, we discovered $Cs_3REGe_3O_9$ (RE = Pr, Nd, and Sm−Yb), a family of germanates that crystallize in a new structure type and have no compositionally analogous silicates. Surprisingly, the Tb flux growth reaction also produced $Cs_8Tb_3Ge_9O_{27}$, a mixed-valent Tb(III)/Tb(IV) oxide. Herein, we report the syntheses, structures, optical properties, and magnetic properties of $Cs_3REGe_3O_9$ and $Cs_8Tb_3Ge_9O_{27}$.

Received: April 9, 2019

DOI: 10.1021/acs.inorgchem.9b01033
Inorg. Chem. XXXX, XXX, XXX−XXX

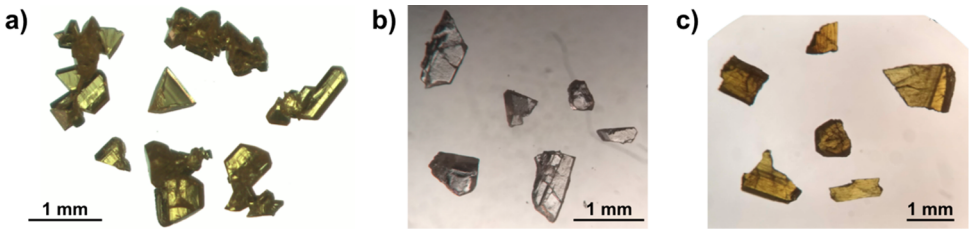

Figure 1. Single crystals of (a) $Cs_3PrGe_3O_9$, (b) $Cs_3DyGe_3O_9$, and (c) $Cs_8Tb_3Ge_9O_{27}$.

EXPERIMENTAL SECTION

Reagents. RE_2O_3 (RE = Nd, Sm–Gd, and Dy–Yb) (99.9%, metal basis, Alfa Aesar), CsCl (99.9%, VWR), CsF (99.9%, Alfa Aesar), and GeO_2 (99.9%, BeanTown Chemical) were used as received with no further modifications. Tb_4O_7 and Pr_6O_{11} (99.9%, metal basis, Alfa Aesar) were reduced to Tb_2O_3 and Pr_2O_3 under a flow of 5% hydrogen in nitrogen gas in a tube furnace at 800 or 1000 °C, respectively, for 12 h. The purities of the synthesized rare earth oxides were confirmed via powder X-ray diffraction (PXRD) data (vide infra).

Synthesis. All compounds were synthesized by molten flux crystal growth with a CsCl/CsF flux. $Cs_3REGe_3O_9$ (RE = Pr, Nd, and Sm–Tm) and $Cs_8Tb_3Ge_9O_{27}$ were synthesized by layering a mixture of 11 mmol of CsCl and 9 mmol of CsF over a mixture of 2 mmol of GeO_2 and 0.5 mmol of RE_2O_3. The mixtures were placed in either a 14 mL high-form silver crucible or a cylindrical silver crucible that is 1.2 cm in diameter and 5.6 cm in height. No differences in reaction products were observed on the basis of the reaction vessel. Both crucibles were loosely covered with a silver lid, heated to 900 °C at a rate of 600 °C/h, held for 12 h, slowly cooled to 400 °C at a rate of 6 °C/h, and rapidly cooled to room temperature by shutting the furnace off. After cooling, the resulting crystals were separated from the solidified flux by dissolving the flux with water aided by sonication for 45–60 min followed by vacuum filtration. $Cs_3YbGe_3O_9$ was synthesized utilizing the conditions described above except in a high-form Pt crucible. Attempts to grow the La analogue of $Cs_3REGe_3O_9$ were unsuccessful. No attempt was made to grow the Ce analogue due to its propensity to oxidize to Ce(IV).

All reactions yielded single crystals of $Cs_3REGe_3O_9$, representative crystals of which are shown in Figure 1, along with other phases. If the Tb reaction is excluded, the identified impurity phases are as follows: $Cs_6RE_2Ge_{11}O_{29}$ (RE = Pr and Nd), $RE_{9.33}(GeO_4)_6O_2$ or a related apatite (RE = Pr, Nd, and Sm),[33] and $RE_2Ge_2O_7$ (RE = Nd and Sm–Yb).[34] The reactions performed in the cylindrical crucibles also produced a large amount of AgCl, which resulted from the flux attacking the tube. This was removed before vacuum filtration by several iterations of swirling the reaction mixture in water under sonication and decanting off the suspended AgCl.

The Tb reaction yielded yellow crystals of $Cs_8Tb_3Ge_9O_{27}$ as the major product (Figure 1c) along with small, colorless crystals of $Cs_3TbGe_3O_9$ and some unidentified phase(s) indicated by PXRD data. Yb reactions performed in Ag reaction vessels did not produce any $Cs_3YbGe_3O_9$ but instead produced a cesium silver ytterbium germanate that appears to crystallize in space group $P1$ with lattice parameters $a \approx 11.23$ Å, $b \approx 11.23$ Å, $c \approx 27.34$ Å, $\alpha \approx 90.42°$, $\beta \approx 90.21°$, and $\gamma \approx 119.89°$ and is comprised of Ge_2O_6 chains connected into a three-dimensional structure by YbO_6-isolated polyhedra and Yb_2O_9 face-sharing dimers. Due to the large, low-symmetry unit cell, combined with poor crystal quality and the presence of twinning, attempts to obtain a publishable crystal structure have so far been unsuccessful. A possible second related compound with similar lattice parameters except for $c \approx 32.81$ Å has also been observed, although the different c axis length may be the result of further twinning. These compounds were also observed in the Tm reaction but were less pervasive.

Samples of $Cs_3REGe_3O_9$ (RE = Pr, Eu, Gd, Dy, and Ho) and $Cs_8Tb_3Ge_9O_{27}$ for the measurement of properties were obtained by manual separation, where the crystals of the desired phase could be distinguished by color (RE = Pr, Tb, and Ho) or morphology (RE = Eu and Gd). PXRD data for the ground samples indicated a small, unidentified impurity in $Cs_8Tb_3Ge_9O_{27}$ (see Figure S1). The remaining samples were phase pure, as indicated by PXRD (Figures S2–S6).

A phase pure sample of $Cs_3TbGe_3O_9$ was synthesized via a solid-state reaction. Extra precautions had to be taken due to the hygroscopic nature of Cs_2CO_3 and the propensity of Tb(III) to partially oxidize to Tb(IV) when heated in air. Stoichiometric amounts of GeO_2 and Cs_2CO_3 (plus 10% extra to account for its evaporative loss at elevated temperatures) were ground in a glovebox for 30 min. To decompose the carbonate, this mixture was placed in an alumina crucible covered by an alumina lid and heated in a furnace at 450 °C for 8 h and 750 °C for 8 h. The reaction mixture was then cooled to 250 °C, at which point the crucible was quickly transferred back into the glovebox to prevent the reaction of any formed Cs_2O with water vapor to form CsOH. The stoichiometric amount of Tb_2O_3 was added, and the mixture was ground for an additional 30 min. The ground powder was loaded into a pellet dye, pressed into a pellet (diameter of 12.5 mm) at a load of ~4.5 t, wrapped in Ag foil, and sealed under vacuum in a flame-dried fused silica tube. The sealed tube was heated to 875 °C, held at this temperature for 48 h, and then cooled back to room temperature by shutting off the furnace. The fused silica tube was attacked by the Cs vapor, which led the tube to crack, presumably during cooling (shorter dwell times or lower dwell temperatures decreased the extent of the attack on the tube and prevented it from cracking but did not result in a phase pure product). The resulting pellet contained some yellow material on its surface, likely an oxidized product that formed after the tube cracked as previous reactions in which the tube survived did not produce any yellow product. This material was removed by sanding the pellet with sandpaper and then sonicating the pellet in acetone to remove the residual SiC powder from the surface. This process produced a phase pure sample of $Cs_3TbGe_3O_9$ as indicated by PXRD data.

Structure. Structure determination for each compound was carried out using single-crystal X-ray diffraction (SXRD) data collected on a Bruker D8 Quest diffractometer equipped with a Mo Kα microfocus source (λ = 0.71073 Å). The raw data were integrated using SAINT+ and corrected for absorption effects using SADABS.[35] An initial structure solution was obtained with SHELXT[36] and refined using SHELXL[37] in the OLEX2 interface.[38] Both $Cs_3REGe_3O_9$ and $Cs_8Tb_3Ge_9O_{27}$ crystallize in noncentrosymmetric space groups and were refined as inversion twins. Crystallographic data for each compound are listed in Table S1.

Powder X-ray diffraction data were collected on a Bruker D2 Phaser equipped with a Cu Kα source (λ = 1.5418 Å). Data were analyzed using the MDI Jade 9 software. Patterns were indexed using reflection data from the ICDD PDF-4+ 2018 database and calculated diffraction patterns based on the CIFs.

Elemental analysis via energy dispersive spectroscopy (EDS) was performed on several analogues of $Cs_3REGe_3O_9$ and $Cs_8Tb_3Ge_9O_{27}$ using data collected on a TESCAN Vega-3 SBU instrument equipped with an EDS detector. Qualitatively, elemental analysis using this data confirmed the presence of each expected element and did not indicate the presence of any other elements in the analyzed crystals.

X-ray photoelectron spectroscopy (XPS) measurements on $Cs_8Tb_3Ge_9O_{27}$ were performed with a Kratos AXIS Ultra DLD XPS system using a monochromatic Al Kα source that was operated at 15

DOI: 10.1021/acs.inorgchem.9b01033
Inorg. Chem. XXXX, XXX, XXX–XXX

Table 1. Lattice Parameters and Single-Crystal X-ray Diffraction Refinement Statistics for $Cs_3REGe_3O_9$ (RE = Pr, Nd, and Sm−Yb), in Space Group $Pna2_1$, and $Cs_8Tb_3Ge_9O_{27}$, in Space Group $P3$

compound	a (Å)	b (Å)	c (Å)	V (Å^3)	$R_1(F)^a$	$\Delta\rho_{max}$, $\Delta\rho_{min}$
$Cs_3PrGe_3O_9$	14.022(2)	7.2405(12)	12.836(2)	1303.2(4)	0.0215	2.591, −1.874
$Cs_3NdGe_3O_9$	13.9959(5)	7.2281(2)	12.8284(4)	1297.77(7)	0.0254	2.979, −2.105
$Cs_3SmGe_3O_9$	13.9327(12)	7.1921(6)	12.8026(11)	1282.89(19)	0.0283	2.884, −2.152
$Cs_3EuGe_3O_9$	13.9054(4)	7.1723(2)	12.7751(3)	1274.11(6)	0.0189	2.678, −1.822
$Cs_3GdGe_3O_9$	13.8827(3)	7.1594(2)	12.7676(3)	1268.99(5)	0.0196	2.611, −1.956
$Cs_3TbGe_3O_9$	13.8466(4)	7.1375(2)	12.7469(4)	1259.78(6)	0.0274	2.805, −2.545
$Cs_3DyGe_3O_9$	13.8165(5)	7.1204(3)	12.7299(5)	1252.35(9)	0.0243	2.774, −2.259
$Cs_3HoGe_3O_9$	13.7914(3)	7.1054(2)	12.7172(3)	1246.20(5)	0.0290	2.532, −2.494
$Cs_3ErGe_3O_9$	13.7625(4)	7.0903(2)	12.6982(3)	1239.09(6)	0.0180	2.169, −1.352
$Cs_3TmGe_3O_9$	13.7380(6)	7.0731(3)	12.6837(5)	1232.48(9)	0.0171	1.801, −1.280
$Cs_3YbGe_3O_9$	13.7033(4)	7.0545(2)	12.6672(4)	1224.54(6)	0.0247	2.162, −1.906
$Cs_8Tb_3Ge_9O_{27}$	11.2906(4)	11.2906(4)	7.9605(3)	878.83(7)	0.0364	3.049, −3.064

^{a}For $F_o^2 > 2\sigma(F_o^2)$.

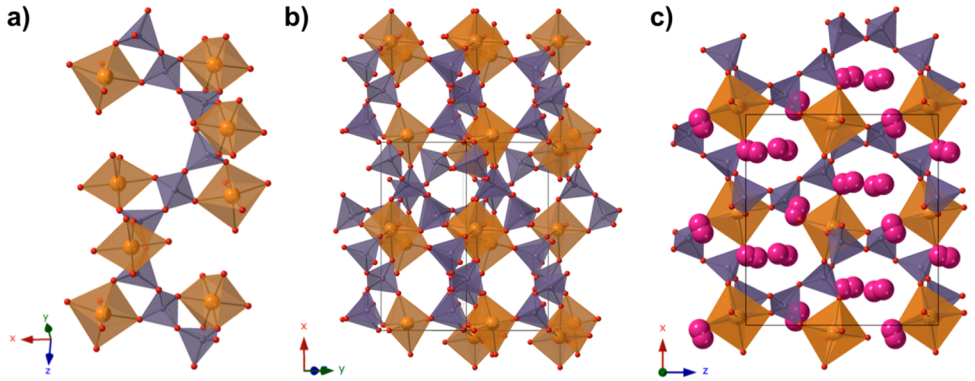

Figure 2. Crystal structure of $Cs_3NdGe_3O_9$ showing (a) a silicate chain, (b) the rare earth germanate framework, and (c) the overall structure. Ge polyhedra are colored gray, Nd polyhedra orange, Cs atoms pink, and oxygen atoms red.

keV and 150 W and a hemispherical energy analyzer. The X-rays were incident at an angle of 45° with respect to the surface normal. Analysis was performed at a pressure of 1×10^{-9} mbar. High-resolution core level spectra were measured with a pass energy of 40 eV, and analysis of the data was carried out using XPSPEAK 41 software.

Properties. Ultraviolet−visible (UV−vis) diffuse reflectance data for $Cs_3TbGe_3O_9$ and $Cs_8Tb_3Ge_9O_{27}$ were collected using a PerkinElmer Lambda 35 UV/vis scanning spectrophotometer equipped with an integrating sphere. Data were collected for the range of 200−900 nm and converted to absorbance using the Kubelka−Munk equation.[39] Fluorescence data for $Cs_3REGe_3O_9$ (RE = Eu and Tb) were collected on a PerkinElmer LS55 luminescence spectrometer. For $Cs_3EuGe_3O_9$, the excitation spectrum was recorded with an emission wavelength of 546 nm and the emission spectrum with an excitation wavelength of 383 nm. For $Cs_3TbGe_3O_9$, the emission and excitation wavelengths were 607 and 235 nm, respectively.

Magnetic measurements on $Cs_3REGe_3O_9$ (RE = Gd, Tb, and Ho) and $Cs_8Tb_3Ge_9O_{27}$ were collected on a Quantum Design SQUID magnetometer (QD MPMS3). Samples of ground single crystals with masses between 15 and 30 mg were massed on a balance sensitive to 0.01 mg and loaded into VSM powder holders. Temperature-dependent susceptibility data were collected from 2 to 300 K at an applied field of 1000 Oe under zero-field-cooled (zfc) and field-cooled (fc) conditions. No deviation was observed between the zfc and fc data. Field-dependent data were collected at 2 K under applied fields of −5 to 5 T. All raw moments were corrected for sample shape and radial offset effects.[40]

RESULTS AND DISCUSSION

Synthesis. Alkali halide fluxes, especially mixed halide fluxes, have been found to be excellent media for the growth of rare earth silicates and germanates.[12,13,41,42] It has been our experience that halide flux reaction mixtures containing a Tb(III) starting material maintain this oxidation state and produce no mixed oxidation state or Tb(IV) products.[43,44] For example, in the case of $Cs_3TbSi_4O_{10}F_2$, which was synthesized at 900 °C from a mixture of $TbCl_3$ and SiO_2 in a CsCl/CsF flux, no difference was observed between the resulting products and the products of reaction mixtures containing a rare earth with only a +3 oxidation state available.[42] Despite the similarities between the syntheses of $Cs_3TbSi_4O_{10}F_2$ and $Cs_8Tb_3Ge_9O_{27}$, the latter reaction readily promotes the oxidation of Tb with $Cs_8Tb_3Ge_9O_{27}$ being the dominant product. This suggests that the germanium plays a role in the formation of Tb(IV) in this reaction, either by catalyzing the oxidation of terbium or by stabilizing the +4 oxidation state once it forms. It is worth noting that the two Tb(IV)-containing oxides synthesized under crystal growth conditions that are not considered highly oxidizing, hydrothermally grown $K_2TbGe_2O_7$ and flux-grown $Cs_8Tb_3Ge_9O_{27}$, are both germanates.[17]

The $Cs_8Tb_3Ge_9O_{27}$ structure type contains Tb(III) and Tb(IV). Among the rare earths, only Ce, Pr, and Tb commonly adopt both the +3 and +4 oxidation states. While the Tb reaction yielded both $Cs_3TbGe_3O_9$ and $Cs_8Tb_3Ge_9O_{27}$, the Pr reaction yielded only $Cs_3PrGe_3O_9$, indicating that either

DOI: 10.1021/acs.inorgchem.9b01033
Inorg. Chem. XXXX, XXX, XXX−XXX

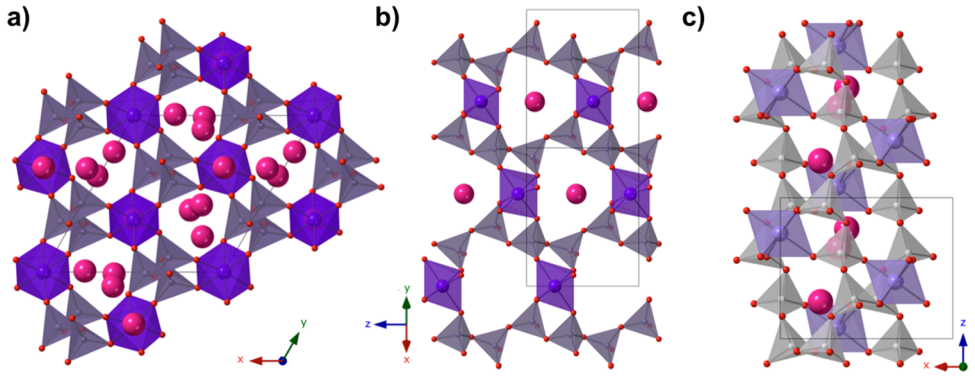

Figure 3. Crystal structure of $Cs_8Tb_3Ge_9O_{27}$ showing (a) the view down the *c*-axis, (b) a view of a slab parallel to the (100) plane, and (c) the arrangement of Cs atoms within the channels. Ge polyhedra are colored gray, Tb polyhedra purple, Cs atoms pink, and oxygen atoms red. Polyhedra are lightened in panel c to make the Cs atoms more visible.

$Cs_8Pr_3Ge_9O_{27}$ does not exist or the Pr was not oxidized to Pr(IV) under our growth conditions. In our experience, Ce completely adopts the +4 oxidation state in a flux growth reaction open to the air, meaning a Ce analogue of $Cs_8Tb_3Ge_9O_{27}$ cannot be grown using the reported conditions. It is possible that the mixed rare earth compounds $Cs_8CeRE_2Ge_9O_{27}$ exist where Ce(IV) occupies the Tb(IV) site and RE(III) occupies the Tb(III) sites (vide infra). A reaction using a stoichiometric mixture of CeO_2 and Dy_2O_3 appeared to produce $Cs_8CeDy_2Ge_9O_{27}$ on the basis of powder diffraction data and unit cell determination via SXRD. However, all of the analyzed crystals were multiply twinned, inhibiting structure solution.

Structure. $Cs_3REGe_3O_9$ compounds crystallize in orthorhombic space group $Pna2_1$ with lattice parameters in the following ranges: a = 13.7033(4)−14.022(2) Å, b = 7.0545(2)−7.2405(12) Å, and c = 12.6672(4)−12.836(2) Å. Lattice parameters for each analogue are listed in Table 1 and follow the trend expected due to lanthanide contraction (see Figure S7). The asymmetric unit contains three cesium sites, a rare earth site, three germanium sites, and nine oxygen sites. The RE atom is coordinated by six oxygen atoms to form an octahedron with bond distances ranging from 2.320 to 2.369 Å, and the germanium atoms are tetrahedrally coordinated by four oxygen atoms with bond distances ranging from 1.711 to 1.781 Å, both for the Nd analogue. The GeO_4 tetrahedra corner-share to form zigzag chains with a Ge_6O_{18} repeating unit (shown in Figure 2a). These chains are connected together into a framework by REO_6 octahedra, which corner-share with two GeO_4 tetrahedra each from three chains (shown in Figure 2b). The connectivity is such that the chains are aligned with chains that are adjacent in the *y*-direction but rotated relative to chains that are adjacent in the *x*-direction. The Cs atoms occupy voids within the structure (shown in Figure 2c). When RE = Pr, Nd, and Sm, disorder is observed in all three unique Cs sites, with one dominant Cs position (occupancy of >80%) and one minor Cs position. For the Eu−Yb analogues, disorder is observed in only two of the Cs sites.

$Cs_8Tb_3Ge_9O_{27}$, shown in Figure 3, crystallizes in space group $P3$ with the following lattice parameters: a = 11.2906(4) Å, and c = 7.9605(3) Å. The asymmetric unit contains three cesium sites, three terbium sites, three germanium sites, and nine oxygen sites. The Tb atoms are coordinated by six oxygen atoms to form octahedra. Tb(1) and Tb(2) have bond distances ranging from 2.261(1) to 2.304(9) Å, whereas Tb(3) has considerably shorter bond distances of 2.141(10)-2.161(10) Å (see Table 2). The bond-valence sums (BVS) for the three sites, calculated using the literature parameters for Tb(III),[45] are 3.10, 2.89, and 4.35, respectively. This suggests that Tb(1) and Tb(2) are trivalent and Tb(3) is tetravalent. Such ordering provides the requisite ratio of oxidation states, $Cs_8Tb^{III}_2Tb^{IV}Ge_9O_{27}$, required for charge balance. The large difference between the assigned oxidation state and BVS for Tb(3) is likely due to the use of Tb(III) bond-valence sum parameters.

Table 2. Terbium Bond Distances and Bond-Valence Sums for $Cs_3TbGe_3O_9$ and $Cs_8Tb_3Ge_9O_{27}$

interaction	$Cs_3TbGe_3O_9$	interaction	$Cs_8Tb_3Ge_9O_{27}$
Tb−O(1)	2.288(7)	Tb(1)−O(3) × 3	2.293(9)
Tb−O(2)	2.314(6)	Tb(1)−O(9) × 3	2.261(10)
Tb−O(4)	2.273(6)	BVS[a]	3.10
Tb−O(5)	2.276(6)	Tb(2)−O(6) × 3	2.300(9)
Tb−O(7)	2.258(7)	Tb(2)−O(8) × 3	2.304(9)
Tb−O(8)	2.306(6)	BVS[a]	2.89
BVS	3.17	Tb(3)−O(4) × 3	2.141(10)
		Tb(3)−O(5) × 3	2.161(10)
		BVS[a]	4.35

[a]Calculated using bond-valence parameters for Tb(III).

As bond-valence parameters have not been reported for Tb(IV), the Tb valence was also analyzed using charge distribution analysis (CHARDI)[46] calculated by CHARDI2015.[47] Whereas BVS rely on a set of empirical parameters determined from known structures, CHARDI uses assigned charges and differences in bond lengths within a single structure to determine bond strengths and, in turn, formal oxidation numbers of each atom. As shown in Table 3, good

Table 3. Assigned Oxidation States (asgnd ox.) and Formal Oxidation Numbers (calc. ox.) Calculated Using CHARDI for Each Tb

	Tb(1)		Tb(2)		Tb(3)	
	asgnd ox.	calc. ox.	asgnd ox.	calc. ox.	asgnd ox.	calc. ox.
all Tb^{3+}	+3	3.07	+3	3.07	+3	3.32
all $Tb^{3.33+}$	+3.33	3.32	+3.33	3.31	+3.33	3.58
all Tb^{4+}	+4	3.77	+3	3.77	+4	4.06
charge ordered	+3	3.07	+3	3.07	+4	4.06

DOI: 10.1021/acs.inorgchem.9b01033
Inorg. Chem. XXXX, XXX, XXX−XXX

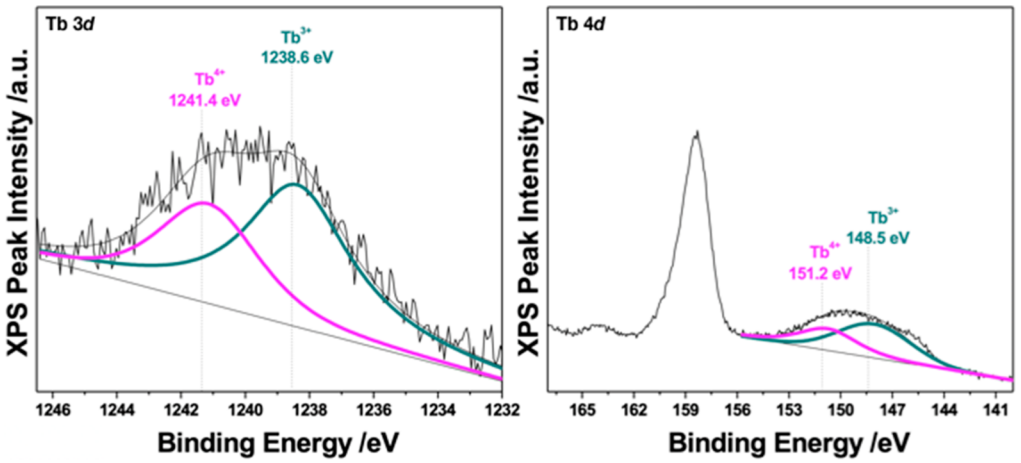

Figure 4. XPS data for $Cs_8Tb_3Ge_9O_{27}$ showing the Tb 3d photoelectron peak (left) and the Tb 4d photoelectron peak (right). The deconvolution into the Tb^{4+} and Tb^{3+} components and the overall fit are shown as pink, teal, and black lines, respectively. The intense peak with a binding energy of ~158 eV is the Cs $4p_{3/2}$ photoelectron peak.

agreement between the assigned and calculated oxidation states of all three Tb sites is achieved only when Tb(1) and Tb(2) are assigned to be +3 and Tb(3) is assigned to be +4. This agrees with the charge distribution suggested by the BVS.

In $Cs_8Tb_3Ge_9O_{27}$, the germanium atoms are tetrahedrally coordinated by oxygen atoms with bond distances ranging from 1.719 to 1.806 Å. The germanium tetrahedra corner-share to form spiral chains with a Ge_3O_9 repeat unit. These chains are connected by TbO_6 octahedra into a framework with the same connectivity observed in $Cs_3REGe_3O_9$. However, in $Cs_8Tb_3Ge_9O_{27}$, all of the germanate chains are aligned in the *z*-direction. This creates channels in the *c*-direction in which two of the Cs atoms sit. One of these Cs sites is disordered with a major position [occupancy of 93.8(3)%] and a minor position. The two remaining Cs atoms lie directly between two terbium octahedra.

To confirm the presence of Tb(IV) in $Cs_8Tb_3Ge_9O_{27}$, XPS data were collected. As shown in Figure 4, the Tb 3d and Tb 4d photoelectron peaks are very wide, indicating the presence of more than one oxidation state. These peaks can be deconvoluted into two components each with binding energies of 148.5 and 151.1 eV (Tb 4d) and 1238.6 and 1241.4 eV (Tb 3d). These binding energies are in very good agreement with those previously reported for Tb^{3+} and Tb^{4+} with the higher-energy component of each peak corresponding to Tb^{4+}.[29] Fitting of the deconvoluted peaks provides an oxidation-state composition of 64% Tb(III) and 36% Tb(IV), which is in excellent agreement with the expected values.

Properties. Figure 5 shows the UV−vis spectra for the two Tb analogues. The spectrum for $Cs_3TbGe_3O_9$ is typical of colorless oxides, where the dominant feature is the absorption band at low wavelengths due to the band gap, calculated to be ~3.4 eV. The spectrum for $Cs_8Tb_3Ge_9O_{27}$ exhibits a broad absorption band centered at ~420 nm that corresponds to the absorption of blue and violet light and explains the yellow color of the compound. This is in agreement with other Tb compounds in which both Tb(III)- and Tb(IV)-containing compounds are colorless,[17] whereas mixed-valent Tb compounds are light brown or light orange in color.[25]

Figure 6 shows the luminescence properties of $Cs_3REGe_3O_9$ (RE = Eu and Tb) which are weakly fluorescent and exhibit their characteristic red and green emissions, respectively. The emission spectrum of $Cs_3EuGe_3O_9$ is typical of Eu(III)

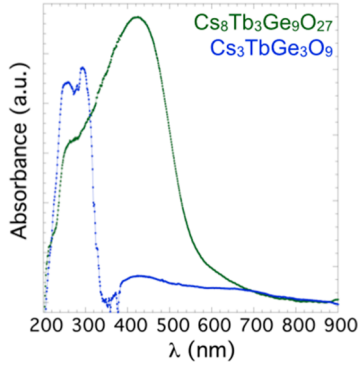

Figure 5. UV−vis spectra of $Cs_3TbGe_3O_9$ (blue) and $Cs_8Tb_3Ge_9O_{27}$ (green).

compounds with the dominant emission peaks at 587 and 607 nm corresponding to the $^5D_0-^7F_1$ and $^5D_0-^7F_2$ transitions, respectively. The high intensity of the latter relative to the prior is indicative of the Eu sitting on a site with no inversion symmetry.[48] The emission spectrum of $Cs_3TbGe_3O_9$ contains four bands with maxima at 482, 546, 574, and 614 nm, corresponding to the $^5D_4-^7F_6$, $^5D_4-^7F_5$, $^5D_4-^7F_4$, and $^5D_4-^7F_3$ transitions, respectively.[48] No luminescence was observed in $Cs_8Tb_3Ge_9O_{27}$.

The magnetic properties of $Cs_3REGe_3O_9$ (RE = Gd, Tb, and Ho) and $Cs_8Tb_3Ge_9O_{27}$ are shown in Figure 7 and summarized in Table 4. All four compounds exhibit paramagnetic behavior with no magnetic ordering down to 2 K. Fitting the high-temperature susceptibility data (50−300 K) with a Curie−Weiss law results in effective moments of 7.73(3) μ_B/Gd, 9.62(3) μ_B/Tb, and 10.55(3) μ_B/Ho for $Cs_3REGe_3O_9$, which are in good agreement with the calculated moments of 7.94(3) μ_B/Gd, 9.72(3) μ_B/Tb, and 10.61(3) μ_B/Ho for the respective trivalent rare earths. The Curie−Weiss fit for $Cs_8Tb_3Ge_9O_{27}$ results in an effective moment of 8.80(3) μ_B/Tb that is somewhat lower than the calculated moment of 9.17 μ_B/Tb for a 2/1 Tb(III)/Tb(IV) mix calculated as the square root of the squared moments times their respective fractions. The low observed moment may be the result of the small, unidentified impurity in the picked sample being nonmagnetic in nature. The field-dependent magnetization for each compound is typical of paramagnetic materials. The

DOI: 10.1021/acs.inorgchem.9b01033
Inorg. Chem. XXXX, XXX, XXX−XXX

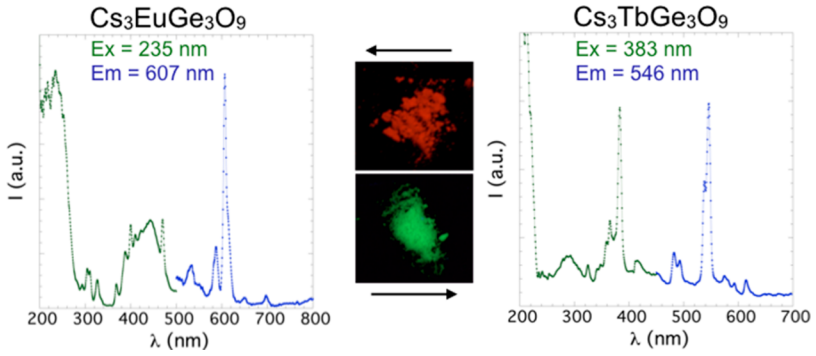

Figure 6. Fluorescence data for $Cs_3EuGe_3O_9$ (left) and $Cs_3TbGe_3O_9$ (right). Optical images of the two analogues under exposure to 254 nm (Eu) or 365 nm (Tb) light are shown in the center.

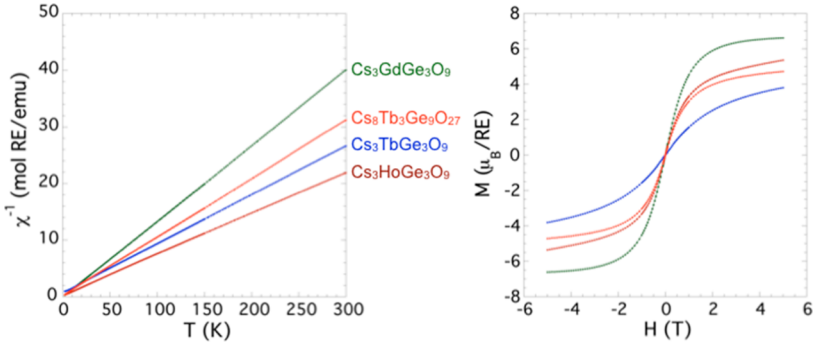

Figure 7. Magnetic properties of $Cs_3REGe_3O_9$ (RE = Gd, Tb, and Ho) and $Cs_8Tb_3Ge_9O_{27}$ showing the inverse susceptibility (left) and magnetization as a function of field (right).

Table 4. Magnetic Properties of $Cs_3REGe_3O_9$ (RE = Gd, Tb, and Ho) and $Cs_8Tb_3Ge_9O_{27}$

	μ_{calc} (μ_B/RE)	θ (K)	μ_{eff} (μ_B/RE)
$Cs_3GdGe_3O_9$	7.94	1.0(3)	7.73(3)
$Cs_3TbGe_3O_9$	9.72	−8.7(3)	9.62(3)
$Cs_3HoGe_3O_9$	10.61	−5.7(3)	10.55(3)
$Cs_8Tb_3Ge_9O_{27}$	9.17	−2.0(3)	8.80(3)

magnetization of $Cs_3GdGe_3O_9$ reaches 6.61 μ_B/Gd at 5 T, close to the calculated saturation magnetization of 7 μ_B/Gd. The remaining moments of 3.81 μ_B/Tb ($Cs_3TbGe_3O_9$), 5.36 μ_B/Ho ($Cs_3HoGe_3O_9$), and 4.72 μ_B/Tb ($Cs_8Tb_3Ge_9O_{27}$) are considerably less than the calculated saturation magnetizations of 9 μ_B/Tb ($Cs_3TbGe_3O_9$), 10 μ_B/Ho ($Cs_3HoGe_3O_9$), and 8.33 μ_B/Tb ($Cs_8Tb_3Ge_9O_{27}$), indicating that the magnetization does not saturate up to an applied field of 5 T.

CONCLUSIONS

Single crystals of $Cs_3REGe_3O_9$ (RE = Pr, Nd, and Sm−Yb) were grown from a CsCl/CsF flux. The Eu and Tb analogues were each found to be weakly luminescent, exhibiting the typical colors and emission spectra for their respective RE^{3+} ions. Magnetic measurements were performed on $Cs_3REGe_3O_9$ (RE = Gd, Tb, and Ho), and all three analogues exhibited Curie−Weiss behavior down to 2 K.

The Tb flux growth reaction yielded both $Cs_3TbGe_3O_9$ and $Cs_8Tb_3Ge_9O_{27}$, the latter of which is a rare example of a mixed-valent Tb(III)/Tb(IV)-containing oxide. The mixed-valent nature of $Cs_8Tb_3Ge_9O_{27}$ was confirmed by structure solution, BVS, XPS data, and magnetic data. Tb(IV) is considered quite oxidizing in nature and is not usually achieved under common synthetic conditions. As similar reactions using SiO_2 instead of GeO_2 do not yield any Tb(IV)-containing products, this suggests that the germanate plays an important role in oxidizing the Tb_2O_3 starting material or stabilizing the formed Tb(IV). For this reason, further exploration of the terbium germanate phase space is warranted.

ASSOCIATED CONTENT

Supporting Information

The Supporting Information is available free of charge on the ACS Publications website at DOI: 10.1021/acs.inorgchem.9b01033.

Powder X-ray diffraction data, crystallographic data, and plots of the lattice parameters and volume of $Cs_3REGe_3O_9$ as a function of rare earth (PDF)

Accession Codes

CCDC 1909033−1909044 contain the supplementary crystallographic data for this paper. These data can be obtained free of charge via www.ccdc.cam.ac.uk/data_request/cif, or by emailing data_request@ccdc.cam.ac.uk, or by contacting The Cambridge Crystallographic Data Centre, 12 Union Road, Cambridge CB2 1EZ, UK; fax: +44 1223 336033.

AUTHOR INFORMATION

Corresponding Author

*E-mail: zurLoye@mailbox.sc.edu.

ORCID

Gregory Morrison: 0000-0001-9674-9224
Stavros G. Karakalos: 0000-0002-3428-5433
Hans-Conrad zur Loye: 0000-0001-7351-9098

DOI: 10.1021/acs.inorgchem.9b01033
Inorg. Chem. XXXX, XXX, XXX−XXX

Author Contributions

[§]G.M. and N.R.S. contributed equally to this work.

Notes

The authors declare no competing financial interest.

■ ACKNOWLEDGMENTS

Research was conducted by the Center for Hierarchical Wasteform Materials (CHWM), an Energy Frontier Research Center (EFRC). The research was supported by the U.S. Department of Energy, Office of Basic Energy Sciences, Division of Materials Sciences and Engineering, under Award DE SC0016574.

■ REFERENCES

(1) Melcher, C. L.; Schweitzer, J. S. Cerium-doped lutetium oxyorthosilicate: a fast, efficient new scintillator. *IEEE Trans. Nucl. Sci.* **1992**, *39*, 502−505.

(2) Dorenbos, P.; van Eijk, C. W. E.; Bos, A. J. J.; Melcher, C. L. Scintillation and thermoluminescence properties of Lu_2SiO_5: Ce fast scintillation crystals. *J. Lumin.* **1994**, *60*−*61*, 979−982.

(3) Park, J. K.; Kim, C. H.; Park, S. H.; Park, H. D.; Choi, S. Y. Application of strontium silicate yellow phosphor for white light-emitting diodes. *Appl. Phys. Lett.* **2004**, *84*, 1647−1649.

(4) Ferdov, S.; Sá Ferreira, R. A.; Lin, Z. Hydrothermal synthesis, structural investigation, photoluminescence features, and emission quantum yield of Eu and Eu-Gd silicates with apatite-type structure. *Chem. Mater.* **2006**, *18*, 5958−5964.

(5) Kostova, M. H.; Ananias, D.; Paz, F. A. A.; Ferreira, A.; Rocha, J.; Carlos, L. D. Evolution of photoluminescence across dimensionality in lanthanide silicates. *J. Phys. Chem. B* **2007**, *111*, 3576−3582.

(6) Chiang, P.-Y.; Lin, T.-W.; Dai, J.-H.; Chang, B.-C.; Lii, K.-H. Flux synthesis, crystal structure, and luminescence properties of a new europium fluoride-silicate: $K_5Eu_2FSi_4O_{13}$. *Inorg. Chem.* **2007**, *46*, 3619−3622.

(7) Ananias, D.; Ferdov, S.; Paz, F. A. A.; Ferreira, R. A.; Ferreira, A.; Geraldes, C. F. G. C.; Carlos, L. D.; Lin, Z.; Rocha, J. Photoluminescent layered lanthanide silicate nanoparticles. *Chem. Mater.* **2008**, *20*, 205−212.

(8) Kowalchuk, C. M.; Paz, F. A. A.; Ananias, D.; Pattison, P.; Carlos, L. D.; Rocha, J. Photoluminescent microporous lanthanide silicate AV-21 frameworks. *Chem. - Eur. J.* **2008**, *14*, 8157−8168.

(9) Li, Y.-C.; Chang, Y.-H.; Lin, Y.-F.; Chang, Y.-S.; Lin, Y.-J. Synthesis and luminescent properties of Ln^{3+} (Eu^{3+}, Sm^{3+}, Dy^{3+})-doped lanthanum aluminum germanate $LaAlGe_2O_7$ phosphors. *J. Alloys Compd.* **2007**, *439*, 367−375.

(10) Choisnet, J.; Deschanvres, A.; Raveau, B. Evolution structurale de nouveaux germanates et silicates de type wadéite et de structure apparentée. *J. Solid State Chem.* **1973**, *7*, 408−417.

(11) Lin, C.-H.; Chen, C.-S.; Shiryaev, A. A.; Zubavichus, Y. V.; Lii, K.-H. $K_3(U_3O_6)(Si_2O_7)$ and $Rb_3(U_3O_6)(Ge_2O_7)$: A pentavalent-uranium silicate and germanate. *Inorg. Chem.* **2008**, *47*, 4445−4447.

(12) Latshaw, A. M.; Wilkins, B. O.; Morrison, G.; Smith, M. D.; zur Loye, H.-C. $A_5RE_4X[TO_4]_4$ crystal growth: Fluoride flux synthesis of $Na_5Ln_4F[GeO_4]_4$ (Ln = Pr, Nd), the first quaternary germanate oxyfluorides. *J. Solid State Chem.* **2016**, *239*, 200−203.

(13) Morrison, G.; Wilkins, B. O.; Spagnuolo, N. R.; Smith, M. D.; zur Loye, H.-C. Rare earth silicates and germanates crystallizing in the wadeite and related structure types. *J. Solid State Chem.* **2019**, *269*, 51−55.

(14) Playford, H. Y.; Modeshia, D. R.; Barney, E. R.; Hannon, A. C.; Wright, C. S.; Fisher, J. M.; Amieiro-Fonseca, A.; Thompsett, D.; O'Dell, L. A.; Rees, G. J.; Smith, M. E.; Hanna, J. V.; Walton, R. I. Structural characterization and redox catalytic properties of cerium-(IV) pyrochlore oxides. *Chem. Mater.* **2011**, *23*, 5464−5473.

(15) Lin, J.; Diwu, J.; Cross, J. N.; Villa, E. M.; Albrecht-Schmitt, T. E. Cerium(IV) tellurite halides $[Ce_2Te_7O_{17}]X_2$ (X = Cl^- or Br^-): The First Cerium-Containing Cationic Frameworks. *Inorg. Chem.* **2012**, *51*, 10083−10085.

(16) Abeysinghe, D.; Gerke, B.; Morrison, G.; Hsieh, C. H.; Smith, M. D.; Pöttgen, R.; Makris, T. M.; zur Loye, H.-C. Synthesis, characterization, and properties of reduced europium molybdates and tungstates. *J. Solid State Chem.* **2015**, *229*, 173−180.

(17) Fulle, K.; Sanjeewa, L. D.; McMillen, C. D.; Wen, Y.; Rajamanthrilage, A. C.; Anker, J. N.; Chumanov, G.; Kolis, J. W. One-pot hydrothermal synthesis of $Tb^{III}{}_3(GeO_4)_6O_7(OH)$ and $K_2Tb^{IV}Ge_2O_7$: Preparation of a stable terbium(4+) complex. *Inorg. Chem.* **2017**, *56*, 6044−6047.

(18) Baenziger, N.; Eick, H.; Schuldt, H.; Eyring, L. Terbium oxides. III. X-ray diffraction studies of several stable phases. *J. Am. Chem. Soc.* **1961**, *83*, 2219−2223.

(19) Wolf, R.; Hoppe, R. Über Na_2PrO_3 und Na_2TbO_3. *Z. Anorg. Allg. Chem.* **1988**, *556*, 97−108.

(20) Tezuka, K.; Hinatsu, Y.; Shimojo, Y.; Morii, Y. Study on the crystal and magnetic structures of and by powder neutron diffraction. *J. Phys.: Condens. Matter* **1998**, *10*, 11703−11712.

(21) Doi, Y.; Wakeshima, M.; Hinatsu, Y.; Tobo, A.; Ohoyama, K.; Yamaguchi, Y. Magnetic and calorimetric studies on 6H-perovskite $Ba_3TbRu_2O_9$. *J. Alloys Compd.* **2002**, *344*, 166−169.

(22) Guillot, M.; El-Ghozzi, M.; Avignant, D.; Andre, G.; Bouree, F.; Cousson, A. Magnetic properties of a mixed-valence (III/IV) terbium fluoride KTb_3F_{12}. *J. Appl. Phys.* **2002**, *91*, 8519−8521.

(23) Largeau, E.; El-Ghozzi, M.; Avignant, D.; Guillot, M.; Bourée, F.; André, G.; Cousson, A. Antiferromagnetic ordering in the KTb_3F_{12} mixed-valence (III/IV) terbium fluoride studied by neutron diffraction and magnetic measurements. *J. Magn. Magn. Mater.* **2003**, *261*, 93−104.

(24) Josse, M.; Dubois, M.; El-Ghozzi, M.; Avignant, D. Synthesis and crystal structure of $Rb_2AlTb_3F_{16}$: a new mixed-valence terbium fluoride. *Solid State Sci.* **2003**, *5*, 1141−1148.

(25) Josse, M.; Dubois, M.; El-Ghozzi, M.; Avignant, D. Synthesis and crystal structures of new mixed-valence terbium (III/IV) fluorides with a random distribution between Tb3+ and Tb4+. *J. Alloys Compd.* **2004**, *374*, 213−218.

(26) Vratny, F. Reflectance spectra of terbium oxides in the range Tb_2O_3 to Tb_4O_7. *J. Chem. Phys.* **1961**, *34*, 1377−1379.

(27) Baenziger, N. C.; Eick, H. A.; Schuldt, H. S.; Eyring, L. Terbium oxides. III. X-ray diffraction studies of several stable phases. *J. Am. Chem. Soc.* **1961**, *83*, 2219−2223.

(28) Glätzle, M.; Janka, O.; Svitlyk, V.; Chernyshov, D.; Bartsch, M.; Zacharias, H.; Pöttgen, R.; Huppertz, H. The high-pressure oxide Tb_3O_5 and its non-centrosymmetric low-temperature polymorph−A comprehensive study. *Chem. - Eur. J.* **2018**, *24*, 15236−15245.

(29) Farid, M. A.; Zhang, H.; Yang, A.; Tian, G.; Wu, M.; Li, G.; Liao, F.; Lin, J. Facile synthesis, structure elucidation, and magnetic properties of perovskite $BaTb_{1-x}Bi_xO_3$. *Eur. J. Inorg. Chem.* **2017**, *2017*, 1427−1434.

(30) Hughey, K.; Yeon, J.; zur Loye, H.-C. Crystal growth and structure determination of the new neodymium germanate, $Na_5Nd_4Ge_4O_{16}(OH)$. *J. Chem. Crystallogr.* **2014**, *44*, 376−379.

(31) Yeon, J.; Hardaway, J. B.; Sefat, A. S.; Latshaw, A. M.; zur Loye, H.-C. Crystal growth, structures, magnetic and photoluminescent properties of $NaLnGeO_4$ (Ln = Sm, Eu, Gd, Tb). *Solid State Sci.* **2014**, *34*, 24−30.

(32) Henshaw, D. E. The structure of wadeite. *Mineral. Mag. J. Mineral. Soc.* **1955**, *30*, 585−595.

(33) Abram, E. J.; Kirk, C. A.; Sinclair, D. C.; West, A. R. Synthesis and characterisation of lanthanum germanate-based apatite phases. *Solid State Ionics* **2005**, *176*, 1941−1947.

(34) Becker, U. W.; Felsche, J. Phases and structural relations of the rare earth germanates $RE_2Ge_2O_7$, RE ≡ La-Lu. *J. Less-Common Met.* **1987**, *128*, 269−280.

(35) *APEXIII* version 2016.5-0, *SAINT* version 7.60A, and *SADABS* version 2016/2; Bruker Analytical X-ray Systems: Madison, WI, 2016.

DOI: 10.1021/acs.inorgchem.9b01033
Inorg. Chem. XXXX, XXX, XXX−XXX

(36) Sheldrick, G. SHELXT - Integrated space-group and crystal-structure determination. *Acta Crystallogr., Sect. A: Found. Adv.* **2015**, *71*, 3−8.
(37) Sheldrick, G. M. A short history of SHELX. *Acta Crystallogr., Sect. A: Found. Crystallogr.* **2008**, *64*, 112−122.
(38) Dolomanov, O. V.; Bourhis, L. J.; Gildea, R. J.; Howard, J. A. K.; Puschmann, H. OLEX2: A complete structure solution, refinement and analysis program. *J. Appl. Crystallogr.* **2009**, *42*, 339−341.
(39) Kubelka, P.; Munk, F. Z. An article on optics of paint layers. *Technol. Phys.* **1931**, *12*, 593−601.
(40) Morrison, G.; zur Loye, H.-C. Simple correction for the sample shape and radial offset effects on SQUID magnetometers: Magnetic measurements on Ln_2O_3 (Ln = Gd, Dy, Er) standards. *J. Solid State Chem.* **2015**, *221*, 334−337.
(41) Latshaw, A. M.; Morrison, G.; zur Loye, K. D.; Myers, A. R.; Smith, M. D.; zur Loye, H.-C. Intrinsic blue-white luminescence, luminescence color tunability, synthesis, structure, and polymorphism of $K_3YSi_2O_7$. *CrystEngComm* **2016**, *18*, 2294−2302.
(42) Morrison, G.; Latshaw, A. M.; Spagnuolo, N. R.; zur Loye, H.-C. Observation of intense X-ray scintillation in a family of mixed anion silicates, $Cs_3RESi_4O_{10}F_2$ (RE = Y, Eu−Lu), obtained via an enhanced flux crystal growth technique. *J. Am. Chem. Soc.* **2017**, *139*, 14743−14748.
(43) Latshaw, A. M.; Wilkins, B. O.; Hughey, K. D.; Yeon, J.; Williams, D. E.; Tran, T. T.; Halasyamani, P. S.; zur Loye, H.-C. $A_5RE_4X[TO_4]_4$ crystal growth and photoluminescence. Fluoride flux synthesis of sodium and potassium rare earth silicate oxyfluorides. *CrystEngComm* **2015**, *17*, 4654−4661.
(44) Latshaw, A. M.; Chance, W. M.; Trenor, N.; Morrison, G.; Smith, M. D.; Yeon, J.; Williams, D. E.; zur Loye, H.-C. $A_5RE_4X[TO_4]_4$ crystal growth and photoluminescence. Hydroflux synthesis of sodium rare earth silicate hydroxides. *CrystEngComm* **2015**, *17*, 4691−4698.
(45) Brown, I. D.; Altermatt, D. Bond-valence parameters obtained from a systematic analysis of the Inorganic Crystal Structure Database. *Acta Crystallogr., Sect. B: Struct. Sci.* **1985**, *41*, 244−247.
(46) Hoppe, R.; Voigt, S.; Glaum, H.; Kissel, J.; Müller, H. P.; Bernet, K. A new route to charge distributions in ionic solids. *J. Less-Common Met.* **1989**, *156*, 105−122.
(47) Nespolo, M.; Guillot, B. CHARDI2015: charge distribution analysis of non-molecular structures. *J. Appl. Crystallogr.* **2016**, *49*, 317−321.
(48) Blasse, G.; Grabmaier, B. C. *Luminescent Materials*; Springer: Berlin, 1994.

DOI: 10.1021/acs.inorgchem.9b01033
Inorg. Chem. XXXX, XXX, XXX−XXX